Journal of Rock Mechanics and Geotechnical Engineering 13 (2021) 1173–1181

Contents lists available at ScienceDirect

Journal of Rock Mechanics and Geotechnical Engineering

journal homepage: www.jrmge.cn

Full Length Article

Consolidation of soft clay foundation improved by geosynthetic-reinforced granular columns: Numerical evaluation

Nima R. Alkhorshid [a,*], Gregório L.S. Araujo [b], Ennio M. Palmeira [b]

[a] Institute of Integrated Engineering, Federal University of Itajubá – Itabira Campus, Itabira, Minas Gerais, 35903-087, Brazil
[b] Department of Civil and Environmental Engineering, University of Brasília, Brasília, Distrito Federal, 70910-900, Brazil

ARTICLE INFO

Article history:
Received 29 November 2020
Received in revised form
25 December 2020
Accepted 7 March 2021
Available online 20 April 2021

Keywords:
Geosynthetic
Embankment
Granular column
Consolidation
Soft soil

ABSTRACT

Soft clays are problematic soils as they present high compressibility and low shear strength. There are several methods for improving in situ conditions of soft clays. Based on the geotechnical problem's geometry and characteristics, the in situ conditions may require reinforcement to restrain instability and construction settlements. Granular columns reinforced by geosynthetic material are widely used to reduce settlements of embankments on soft clays. They also accelerate the consolidation rate by reducing the drainage path's length and increasing the foundation soil's bearing capacity. In this study, the performance of encased and layered granular columns in soft clay is investigated and discussed. The numerical results show the significance of geosynthetic stiffness and the column length on the embankment settlements. Furthermore, the results show that granular columns may play an important role in dissipating the excess pore water pressures and accelerating the consolidation settlements of embankments on soft clays.

1. Introduction

Granular columns are widely used in geotechnical engineering to reduce settlement, increase bearing capacity, accelerate consolidation, and decrease liquefaction potential. Based on the surrounding soil's lateral confinement, the required granular columns' strength and stiffness may be determined (Zhang et al., 2013). Due to low shear strength presented by very soft soils, granular columns in such soils are not suggested. This issue can be solved by lateral support of the column material using geosynthetic encasement. In the recent past, geotextile has been used for encasing granular columns in very soft soils. Geotextile provides confinement around the columns and behaves as drainage and filter boundary, yielding less contamination of the sand core with soft soil particles (Castro and Sagaseta, 2011; Zhang et al., 2012; Pulko and Logar, 2017; Chen et al., 2020; Li et al., 2020). Geogrid may be a stiffer alternative to geotextile (Araujo et al., 2009; Gniel and Bouazza, 2009; Murugesan and Rajagopal, 2010; Gu et al., 2016), but it cannot avoid the sand core contamination.

Recently, various field and laboratory works have been carried out to evaluate geosynthetic-encased granular column's performance (De Mello et al., 2008; Alexiew and Raithel, 2015; Xue et al., 2019; Chen et al., 2020). The granular column's application has experienced different designs such as partial and full encasement (Ali et al., 2012; Yoo and Lee, 2012; Alkhorshid, 2017; Alkhorshid et al., 2020; Cengiz and Guler, 2020; Zhang et al., 2020), floating conventional and encased columns (Ali et al., 2014; Rathod et al., 2020), and a few laboratory tests on geosynthetic-layered columns (Sharma et al., 2004) which are non-encased columns reinforced by geosynthetic disks within their inner region.

Finite element method (FEM) has been extensively used to evaluate the behavior of encased granular columns (Khabbazian et al., 2010; Alkhorshid, 2012; Alkhorshid et al., 2014; Keykhosropur et al., 2012; Castro and Sagaseta, 2013; Mohapatra et al., 2017; Nagula et al., 2018; Hosseinpour et al., 2019). However, encased granular columns are considered as a new method for supporting embankments and need to be investigated to understand their behavior and to improve design methods. In this numerical study, finite element analyses have been carried out using PLAXIS 2D to study the influence of granular column design approach on its performance. Besides partially encased, fully encased end-bearing, and floating columns, a new approach was

* Corresponding author.
E-mail address: nimara@unifei.edu.br (N.R. Alkhorshid).
Peer review under responsibility of Institute of Rock and Soil Mechanics, Chinese Academy of Sciences.

https://doi.org/10.1016/j.jrmge.2021.03.004

taken to reinforce the granular column. In this approach, the column is partly encased and partly layered with geosynthetic.

2. Modeling with PLAXIS 2D

2.1. Proposed model

The displacement method is commonly used as the installation method of granular columns in very soft soils (Alexiew et al., 2005; Gniel and Bouazza, 2009). It is carried out either by a static or jointly by a static and dynamic installation that causes cylindrical soil densification (Fig. 1) around the column (smear zone), which changes the value of the coefficient of lateral earth pressure (K). As reported by Priebe (1995) and Gäb et al. (2008), this coefficient can be assumed as $K = 1$, and Goughnour and Bayuk (1979) took this coefficient as $K_0 < K < K_p$, where K_0 and K_p are the coefficients of earth pressure at rest and the passive earth pressure of the soil, respectively. Walker and Indraratna (2006) stated that the radius of the smear zone (r_s) could be estimated as 2–3 times the radius of the column (r_c). Weber (2008) assumed r_s as twice r_c, and Wang (2009) assumed r_s to be 1–2 times r_c and k_s/k_h equals 0.1, where k_s and k_h are the coefficient of permeability of the smear zone and horizontal coefficient of permeability of the soil, respectively. Alkhorshid (2017) and Alkhorshid et al. (2019) carried out a series of large-scale laboratory tests and measured the smear zone's radius as 1.8–1.9 times the column diameter. The unit cell concept (Fig. 1) was adopted to represent a cylindrical column-soil system with a radius equal to the radius of the column influence zone (r_e). Several researchers have used the unit cell concept to evaluate soft soil reinforcement with encased columns (e.g. Murugesan and Rajagopal, 2007; Almeida et al., 2013; Rajesh, 2017; Gholaminejad et al., 2020).

2.2. Hardening soil (HS) model

Hardening soil (HS) model is a development on the Mohr-Coulomb (MC) model that associates the nonlinear elastic model to the elastoplastic model. This model can simulate the behavior of both soft and stiff soils. More information on this model is presented in Schanz (1998) and Schanz et al. (1999).

2.3. Axisymmetric model

The performance of geosynthetic-encased end-bearing and floating granular columns and the geosynthetic-layered granular columns was analyzed by the finite element program PLAXIS 2D. The vertical displacements are allowed in the unit cell boundaries (Figs. 2 and 3). The horizontal displacements at the sides (roller boundary condition) and the vertical and horizontal displacements at the base were fixed.

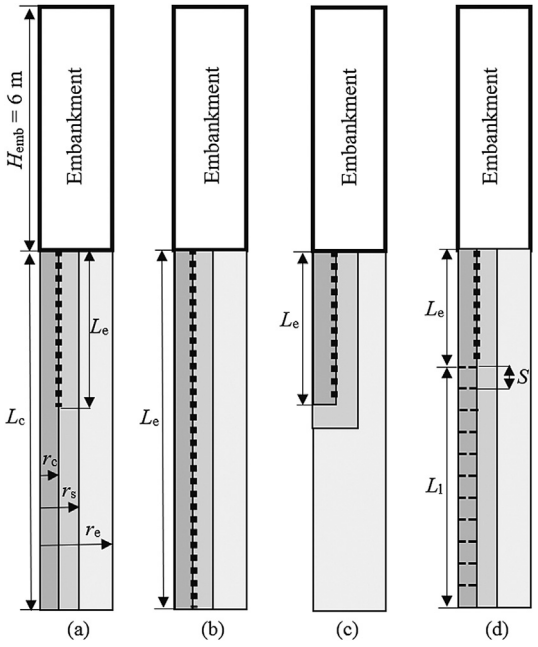

Fig. 2. Axisymmetric modeling: (a) Partial encasement, (b) Full encasement, (c) Fully encased floating column, and (d) Combination of encasement and layering (disks of geogrid).

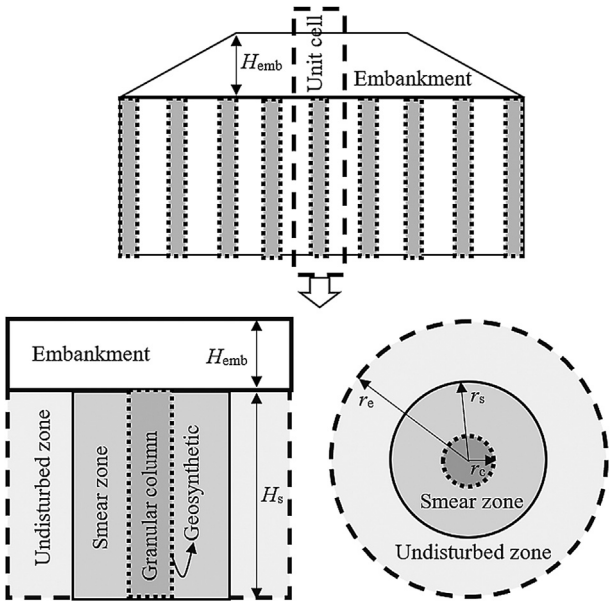

Fig. 1. Unit cell idealization. H_s is the thickness of soft soil, and H_{emb} is the embankment height.

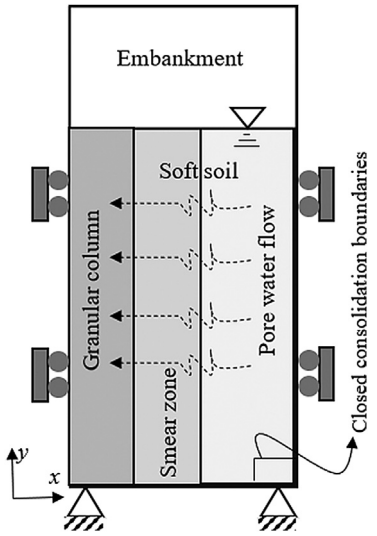

Fig. 3. Boundary conditions of the axisymmetric unit cell.

Table 1
Material parameters in finite element model.

Material property	Soft clay (HS)	Granular column (MC)	Embankment (MC)
Saturated unit weight, γ_{sat} (kN/m^3)	15	19	20
Effective Young's modulus, E' (kPa)	–	45,000	35,000
Effective friction angle, φ' (°)	20	39	25
Dilatancy angle, ψ (°)	0	5	0
Effective cohesion, c' (kPa)	8	0.1	6
Effective Poisson's ratio, ν'	0.2	0.3	0.33
Tangent stiffness for primary oedometer loading, $E_{oed,ref}$ (kPa)	1150	–	–
Coefficient of earth pressure at rest, K_0	0.65	0.37	0.57
Hydraulic conductivity in x-direction, K_x (m/d)	1.38×10^{-4}	3	1
Hydraulic conductivity in y-direction, K_y (m/d)	6.95×10^{-5}	3	1
Power for stress-level dependency of stiffness, m	1	–	–
Reference pressure, P_{ref} (kPa)	100	–	–
Interface coefficient, R_{int}	0.4	0.8	–

As shown in Fig. 2, the encased granular column was studied using full and partial geosynthetic encasement. In the latter case, the length of encasement (L_e) is less than the length of the end-bearing granular column (L_c). In some cases, the column is partly encased (L_e) and partly layered (L_l). The column diameter (d_c) in all cases is equal to 0.8 m. For the case of floating columns, the column was assumed fully encased.

In the analyses, the thickness of soft soil (H_s) is 10 m, the embankment height (H_{emb}) is 6 m, and the smear zone radius (r_s) is assumed as 1.9 times the column radius (r_c = 0.4 m) (Alkhorshid et al., 2019). The HS and MC models were adopted to model soft soil (Schanz, 1998) and granular column, respectively. The geosynthetics were simulated using a linear elastic model with tensile stiffness (J) equal to 2000 kN/m. The interface elements were introduced on the sides of geosynthetics to consider the interaction with soft soil and column material, and the interface coefficient (R_{int}) listed in Table 1 was assigned to take into account this interaction. No tensile failure of the geosynthetic encasement was assumed in the analyses carried out and the constraint provided by the geosynthetic is considered by its tensile stiffness. The permeability of the soil within the smear zone in the horizontal and vertical directions was assumed to be identical and equal to 1.38×10^{-5} m/d (Gäb et al., 2008).

In all cases, coupled consolidation analyses were considered to evaluate the excess pore water pressure and primary consolidation settlement of the granular column and surrounding soil within the column influence zone. The water level was assumed at the soil-column surface, and impervious boundaries were assigned at the boundaries of the unit cell, as shown in Fig. 3. The consolidation calculations were continued until the minimum pore water pressure (less than 1 kPa) was accomplished. The properties of the soil, column fill and embankment used in the parametric analyses are given in Table 1.

2.4. Model calibration for partially, fully encased and conventional columns

Ali (2014) carried out laboratory tests to evaluate the influence of encasement on granular column performance. The soft soil was prepared at a water content of 40% to reach an undrained shear strength of 6–7 kPa. The end-bearing columns consisted of stone grains with a relative density of 60%, resulting in an internal friction angle of 45° obtained from direct shear tests. The columns were installed with a diameter of 50 mm and a length of 450 mm. The results showed that the full encasement significantly contributed to the maximum column failure stress compared to partially encased and conventional columns (hereafter the granular columns without geosynthetic encasement will be referred to as conventional columns). For model calibration in the present study, an axisymmetric unit cell was considered to model partially, fully encased and conventional columns, as shown in Fig. 4. The geotextile had a normal stiffness of 30 kN/m. The properties of the column and soft soil used in the calibration are given in Table 2. The parameters used for model calibration were obtained from the properties provided by the previous studies (e.g. Oh et al., 2007; Ali, 2014; Alkhorshid et al., 2019) and using the soil test tool in PLAXIS 2D and

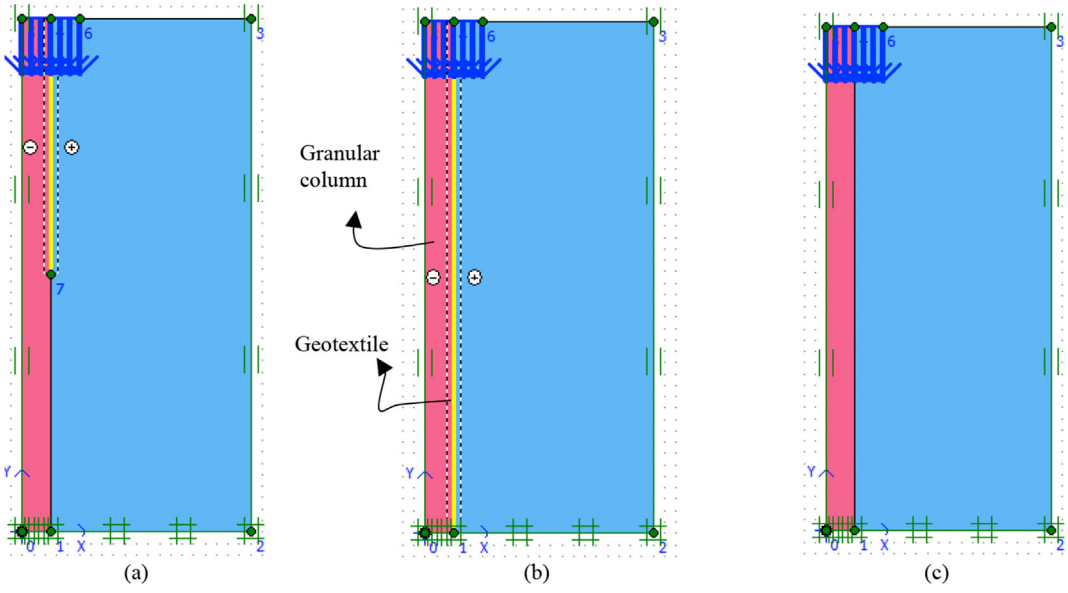

Fig. 4. Model calibration: (a) Partially encased column, (b) Fully encased column, and (c) Conventional column.

Table 2
Material properties assumed by the present study for model calibration of encased and conventional columns.

Material property	Soft clay (HS)	Stone column (MC)
γ_{sat} (kN/m^3)	18.59	19
E' (kPa)	–	6500
φ' (°)	20	45
ψ (°)	0	3
c' (kPa)	5	0.1
ν'	0.2	0.33
$E_{oed,ref}$ (kPa)	350	–
m	1	–
P_{ref} (kPa)	100	–

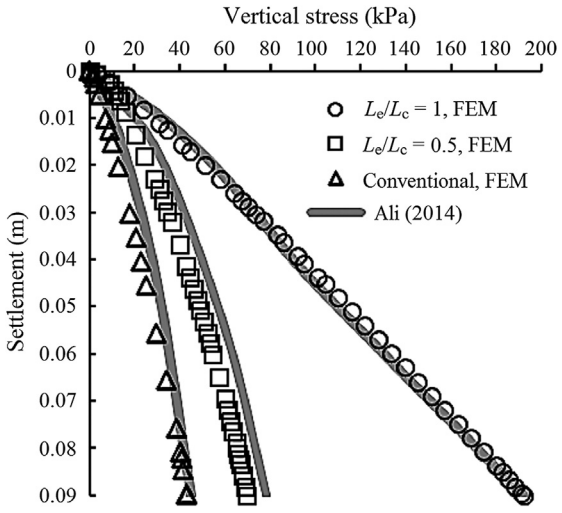

Fig. 5. Model calibration for encased and conventional columns.

back analysis. As shown in Fig. 5, the numerical (FEM) analysis results compared well with those of laboratory tests.

2.5. Model calibration for consolidation of soft soil improved by granular column

Oh et al. (2007) presented a study on a trial embankment on soft soil (undrained shear strength S_u = 5–20 kPa) improved by granular columns with the spacings of 2 m and 3 m in a square pattern. The results showed that the columns with 2 m spacing underwent less settlement than those of 3 m spacing and those of the embankment with no ground improvement. An axisymmetric unit cell model (Fig. 6) was used to verify the column consolidation settlements. The properties of materials used to model field tests in the present study are presented in Table 3. The results obtained from the numerical analysis are in fair agreement with those of the field tests (Fig. 7).

2.6. Model calibration for dissipation of excess pore water pressure

Alkhorshid et al. (2019) carried out a series of large-scale laboratory tests to evaluate column installation and behavior in a very soft soil (S_u = 2 kPa). The study adopted the displacement installation method for column execution. Two piezometers were installed close to the column at the bottom of the test tank to measure the excess pore water pressure due to the column installation in the soft soil. The displacement installation method was

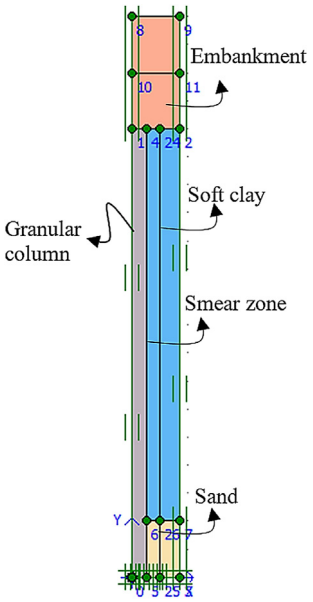

Fig. 6. Model calibration of a trial embankment.

Table 3
Material properties assumed by the present study for model calibration of a trial embankment.

Material property	Soft clay (HS)	Granular column (MC)	Embankment (MC)	Sand (MC)
γ_{sat} (kN/m^3)	15	18	20	17
E' (kPa)	–	30,000	25,000	120,000
φ' (°)	20	38	25	33
ψ (°)	0	5	0	3
c' (kPa)	10	0.1	10	0.1
ν'	0.2	0.3	0.3	0.3
$E_{oed,ref}$ (kPa)	1150	–	–	–
K_x (m/d)	1.38×10^{-4}	3	1	1
K_y (m/d)	6.95×10^{-5}	3	1	1
m	1	–	–	–
P_{ref} (kPa)	100	–	–	–

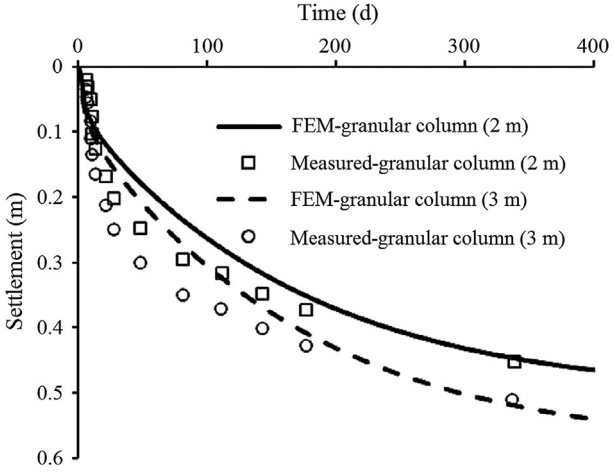

Fig. 7. Model calibration for consolidation settlement.

modeled by causing a cavity expansion (Castro and Karstunen, 2010) using prescribed lateral displacements (Fig. 8). The

properties of the soil used in the FEM are given in Table 4. The results obtained from the FEM compared reasonably well with those from the tests, as shown in Fig. 9.

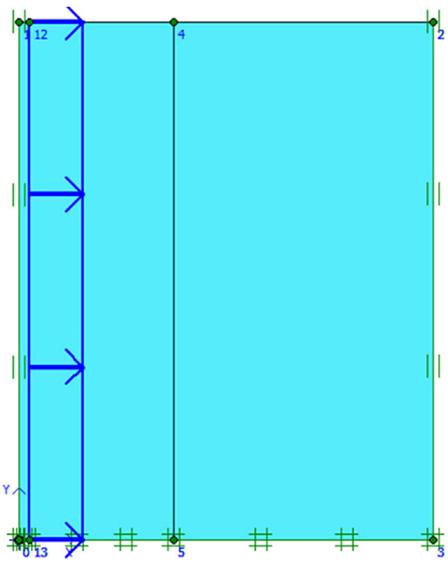

Fig. 8. Model calibration for the displacement installation method.

Table 4
Soft soil parameters used in FEM simulation.

Material property	Value
γ_{sat} (kN/m^3)	17
φ' (°)	25
ψ (°)	0
c' (kPa)	4
ν'	0.2
$E_{oed,ref}$ (kPa)	500
K_x (m/d)	1.39×10^{-3}
K_y (m/d)	1.39×10^{-3}
m	1
P_{ref} (kPa)	100

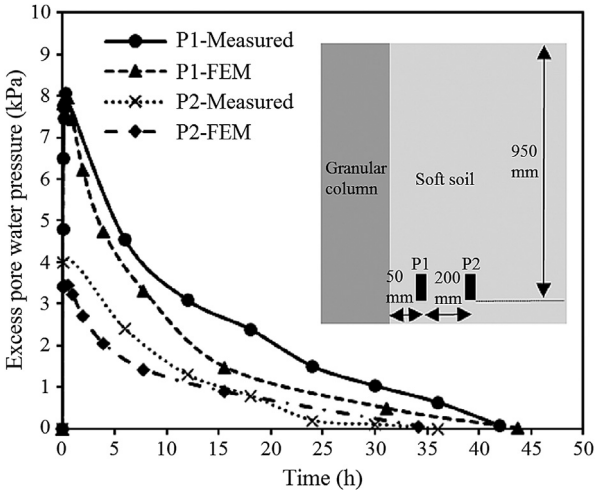

Fig. 9. Model calibration for the dissipation of excess pore water pressure.

3. Parametric study

In parametric study, the results of the fully encased floating column, as well as the results of the partial encasement and the combination of encasement and layering of the end-bearing column, are presented and discussed. In this study, the geotextile stiffness (J) and the diameter ratio ($N = d_e/d_c$, where d_e is the column influence zone diameter and d_c is the column diameter) are equal to 2000 kN/m and 2.5, respectively, except for the cases in which these values (J and N) are considered as variables.

3.1. Fully encased floating column

Fig. 10 shows that the floating ratio ($\rho = L_e/H_s$) has an essential role in the settlements experienced by the column and surrounding soil, since the smallest settlements were obtained for $\rho = 1$ (encased end-bearing column) which showed an improvement of 300% in comparison to the case of $\rho = 0.1$. On the other hand, as ρ grows, the differential settlements increase so that the smallest differential settlements are obtained for $\rho = 0.1$ and 0.3.

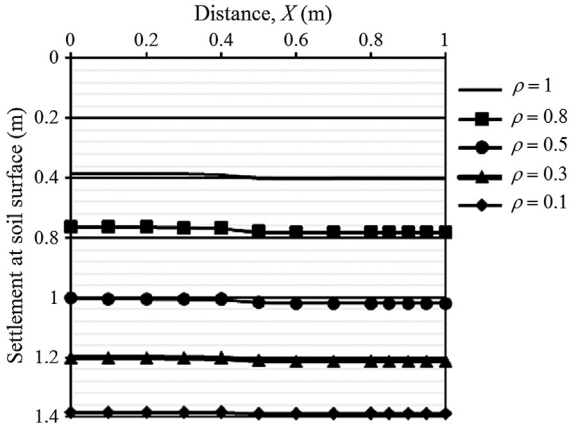

Fig. 10. Settlement at the soil surface for different floating ratios (ρ).

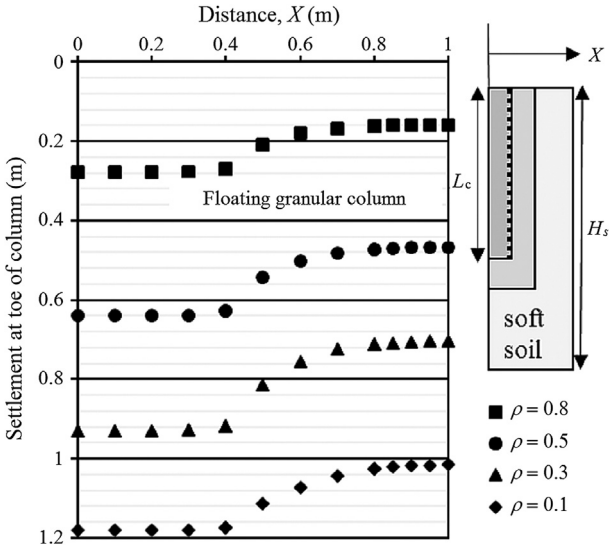

Fig. 11. Settlement (punching settlements) at the column tip for different floating ratios (ρ).

Fig. 11 shows how the floating column can enhance punching settlements of the soft soil when the soil beneath the column tip is not resistant enough to support it or for low values of ρ. By considering the settlements at the soil surface (Fig. 10) and of the column tip (Fig. 11), the column with $\rho = 0.1$ showed higher values of punching settlements than the columns with greater floating ratios. This column ($\rho = 0.1$) exhibited similar settlements at the column top and tip (Figs. 10 and 11), but as the floating ratio increased, the tip settlements became smaller than those at the column top.

Fig. 12 shows the shear strain patterns developed above the encased column. Shear bands on the top of the column and surrounding soil increase in size for increasing values of ρ. This figure also shows a triangular plastification zone at the floating column tip as a consequence of punching settlements. The triangular zone (soil wedge) at the floating column tip becomes more significant as ρ is reduced, which implies that lower values of ρ can enhance the punching settlement mechanism at the column tip.

The variation of the normalized column settlement ($\mu = S_c/H_s$, where S_c is the settlement on the top of the columns) with time is depicted in Fig. 13. The larger the floating ratio, the smaller the consolidation settlement. This figure illustrates that the conventional column presents a better performance than the columns with $\rho = 0.1$, 0.3 and 0.5. When ρ reaches 0.8, the column settlements decrease considerably compared to the end-bearing conventional column. The end-bearing encased column shows a better performance, considering the consolidation time and settlements. The column settlements decrease by factors of 3 and 2 compared to that of the column with $\rho = 0.1$ and the end-bearing conventional column, respectively.

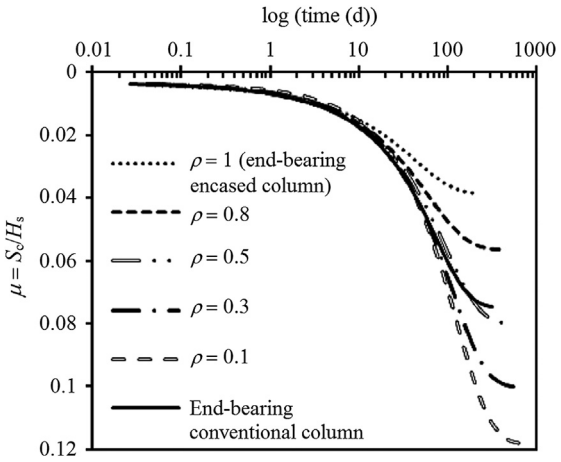

Fig. 13. Settlement at the top of column for different floating ratios.

Point *A* (Fig. 14), located close to the bottom of the soft soil layer, was chosen to evaluate the excess pore water pressure dissipation. Thus, it takes much more time for the system to dissipate the pore water pressure produced at this point. The dissipation of excess pore water pressure (at point *A*) for the column with $\rho = 1$ was improved significantly by 320%, 240% and 180% compared to the columns with $\rho = 0.1$, 0.5 and 0.8, respectively. It shows the effect of the floating factor on radial drainage and, consequently, on reducing drainage paths.

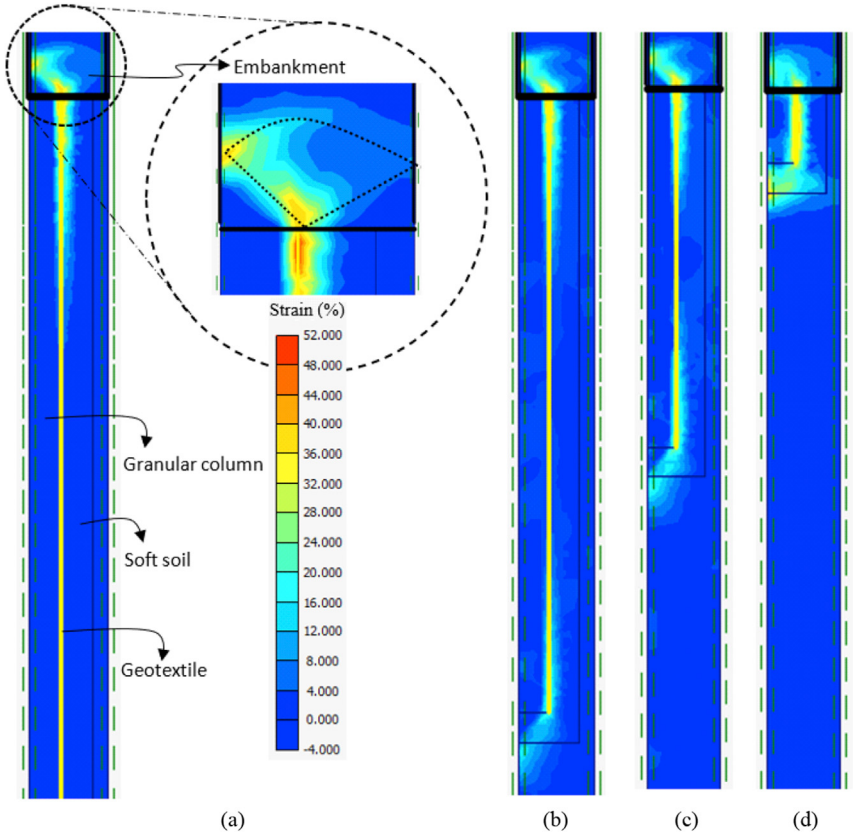

Fig. 12. Shear strain patterns: (a) End-bearing column, (b) Column with $\rho = 0.8$, (c) Column with $\rho = 0.5$, and (d) Column with $\rho = 0.1$.

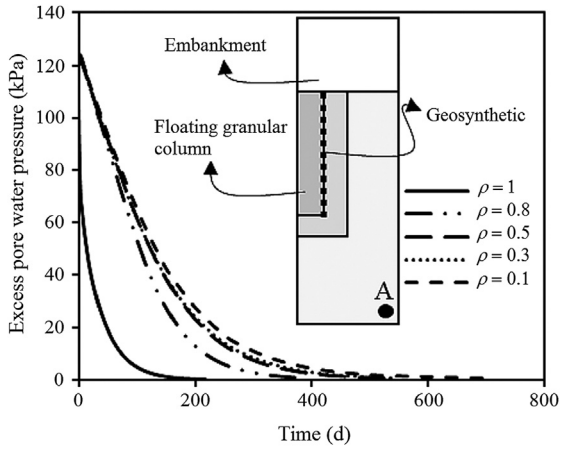

Fig. 14. Dissipation of excess pore water pressure for floating columns.

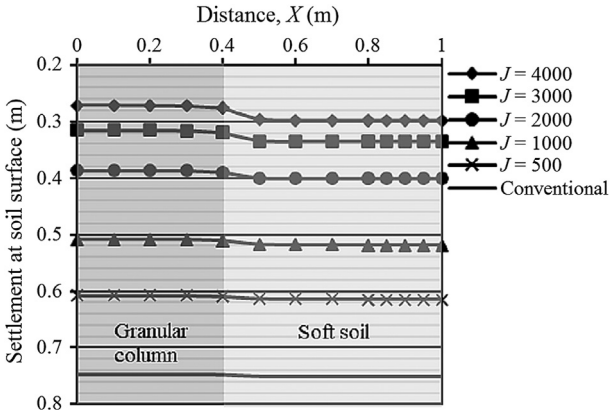

Fig. 16. Settlement at the soil surface for different values of geosynthetic stiffness.

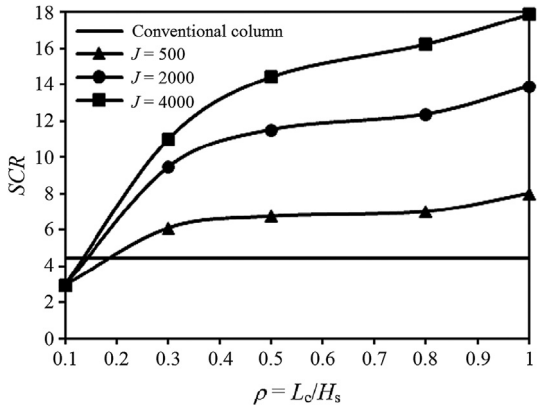

Fig. 15. Stress concentration factor versus floating ratio.

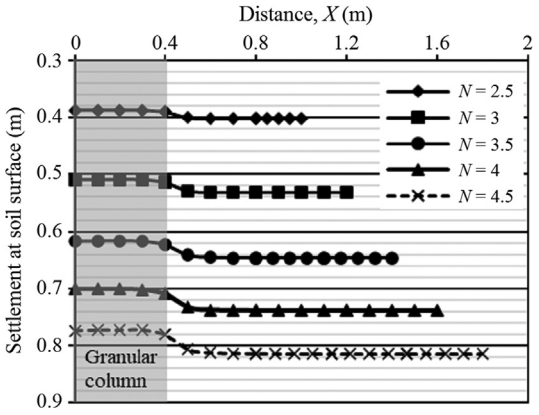

Fig. 17. Settlement at the soil surface for different values of *N*.

Fig. 15 shows the effects of the floating ratio and geosynthetic tensile stiffness (J) on the stress concentration ratio ($SCR = \sigma_{v,c}/\sigma_{v,s}$, where $\sigma_{v,c}$ and $\sigma_{v,s}$ are the vertical stresses supported by the column and surrounding soil, respectively). The stress points considered for the column and surrounding soil were chosen from the points close to the axis of symmetry and the soft soil lateral boundary (at the top of unit cell), respectively. *SCR* for the column with $\rho = 0.1$ is less than that of the conventional column, but as ρ increases to values greater than 0.2, the column becomes capable of carrying higher vertical stresses than those carried by the conventional column. Different studies in the literature showed the importance of the geosynthetic stiffness on column performance (Almeida et al., 2013; Hong et al., 2017; Alkhorshid et al., 2018). By increasing J, *SCR* increases, except for the column with $\rho = 0.1$, for which no improvement can be noted with increasing values of J.

3.2. Partially and fully encased end-bearing columns

As shown in Fig. 16, the surface settlement decreases with increasing encasement tensile stiffness (J). When J reaches 4000 kN/m, the column settlement decreases by a factor of 2.7 compared to that of the conventional column. On the other hand, the differential settlements in between columns increase as J increases, with the highest value of differential settlements being observed for the encased column with $J = 4000$ and the lowest one for the conventional column.

The diameter ratio ($N = d_e/d_c$) directly influences column performance, as shown in Fig. 17. When N increases, both consolidation and differential settlements increase. For $N = 2.5$, both the consolidation and differential settlements are approximately 50% smaller than those for $N = 4.5$ (Fig. 17).

Fig. 18 illustrates the influence of N on the normalized column settlement (μ). It can be noted that it will take more time for significant soft soil consolidation to take place as N increases. N values equal to 2.5 and 4.5 yield the lowest and highest times needed for primary consolidation to be completed, respectively. This is also observed for the dissipation of excess pore water pressure at point A (Fig. 19). As N increases from 2.5 to 4.5, the time required for the dissipation of excess pore water pressure at that point increases by a factor of 5.7.

Fig. 20 shows the settlement reduction factor (β = reinforced column settlement/conventional column settlement) versus time. The length of encasement influences both the consolidation settlement and time. For a length of encasement (L_e) equal to 6 times the diameter of column (d_c) and for the fully encased column, the settlement (for 200 d) decreases by 21% and 43%, respectively, with respect to a value of $L_e = 2d_c$.

The behavior of partially encased columns can be improved by reinforcing the column's uncased portion using geosynthetic disks (layered portion, L_l). For the column partially encased ($6d_c$), by adoption of a distance (S) between two consecutive disks equal to 0.3 m ($S = 0.38d_c$), the column behaves like the fully encased end-

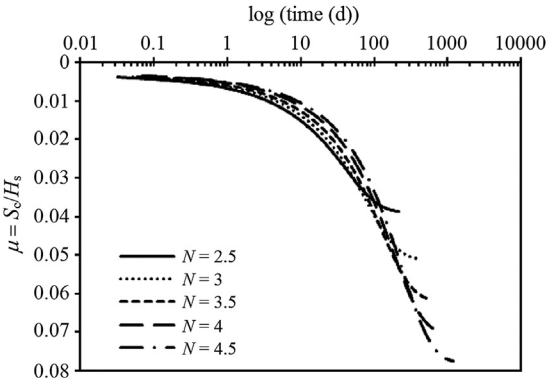

Fig. 18. Settlement at the top of the column for different values of *N*.

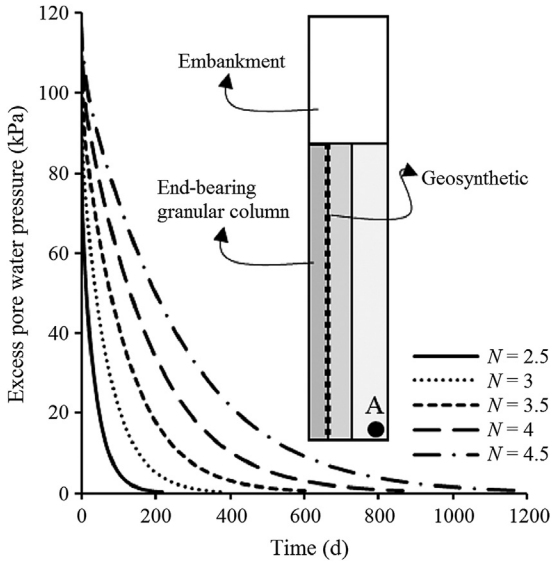

Fig. 19. Dissipation of excess pore water pressure at point *A* for different values of *N*.

bearing one. For this column ($6d_c$), as *S* reduces to values less than $0.38d_c$ (e.g. $S = 0.2$ m), it performs better than the fully encased end-bearing column. Hosseinpour et al. (2014) concluded that the fully layered column settles as equal as the fully encased column when *S* is adopted as $0.25d_c$.

4. Conclusions

In this study, the effects of the floating ratio and the geosynthetic encasement length and type were evaluated using FEM. The conclusions can be drawn as follows:

(1) By increasing the floating ratio (ρ), the differential settlement increases, and consolidation settlement decreases. As the floating ratio increases, the times needed for dissipation of excess pore water pressure and consolidation settlement being accomplished decrease considerably. On the other hand, the reduction of the floating ratio enhances the punching settlements.

(2) In the present study, the column with $\rho = 0.5$ and $J = 2000$ kN/m settles like the conventional column, but the time for consolidation settlement increases by a factor of 1.72 compared to that of the conventional column. On the other hand, the column with $J \geq 500$ kN/m and $\rho > 0.2$ presents greater *SCR* values than the conventional column.

(3) The increases of the tensile stiffness (J) and diameter ratio (N) yield higher values of the differential settlements for the end-bearing encased column. By contrast, the consolidation settlement decreases as J increases and N decreases.

(4) By decreasing N from 4.5 to 2.5 (a difference of 2), the ultimate times needed for dissipation of excess pore water and consolidation settlements of the end-bearing encased column are reduced by factors of 5.7 and 4.6, respectively.

(5) For partially encased columns, as the length of encasement (L_e) increases, the settlement decreases. For the partly encased column with $L_e = 6d_c$ and partly layered (L_l, with $S = 0.38d_c$), the column acts like the fully encased end-bearing one and results in a reduction of 18% of geosynthetic used. Besides, when *S* is reduced to values less than $0.38d_c$, the column produces smaller settlements than the fully encased end-bearing column.

Declaration of competing interest

The authors wish to confirm that there are no known conflicts of interest associated with this publication, and there has been no

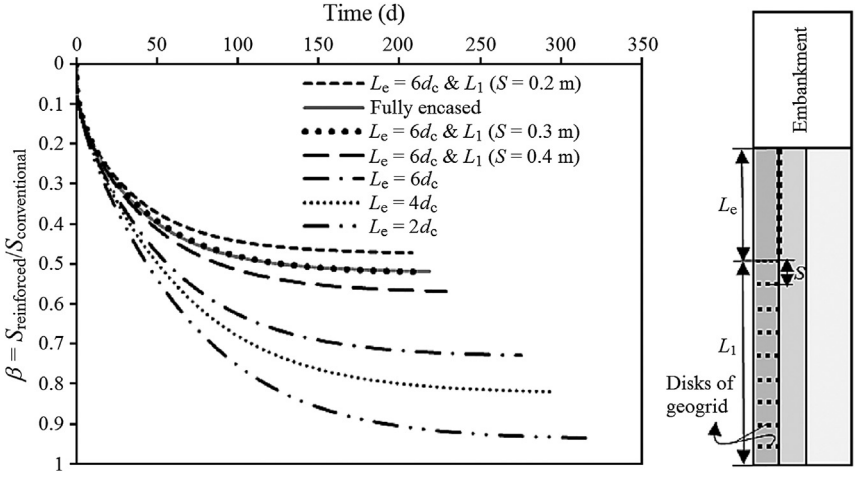

Fig. 20. Settlement reduction factor (β) for different types of column reinforcement.

significant financial support for this work that could have influenced its outcome.

References

Alexiew, D., Raithel, M., 2015. Geotextile-encased columns: case studies over twenty years. In: Indraratna, E.B., Chu, J., Rujikiatkamjorn, C., edited (Eds.), Ground Improvement Case Histories. Elsevier, Kidlington, Oxford, UK.

Alexiew, D., Brokemper, D., Lothspeich, S., 2005. Geotextile encased columns (GEC): load capacity, geotextile selection and pre-design graphs. In: Geo-Frontiers Congress 2005. American Society of Civil Engineers (ASCE), Austin, Texas, USA.

Ali, K., 2014. Effect of encasement length on geosynthetic reinforced stone columns. Int. J. Res. Eng. Tech. 3 (6), 72–75.

Ali, K., Shahu, J.T., Sharma, K.G., 2012. Model tests on geosynthetic-reinforced stone columns: a comparative study. Geosynth. Int. 19 (4), 292–305.

Ali, K., Shahu, J.T., Sharma, K.G., 2014. Model tests on single and groups of stone columns with different geosynthetic reinforcement arrangement. Geosynth. Int. 21 (2), 103–118.

Alkhorshid, N.R., 2012. Numerical Analysis of Soft Clay Reinforced with Stone Columns. MS Thesis. Eastern Mediterranean University, Gazimağusa, North Cyprus.

Alkhorshid, N.R., 2017. Analysis of Geosynthetic Encased Columns in Very Soft Soil. PhD Thesis. Department of Civil and Environmental Engineering, University of Brasilia, Brasilia, Brazil.

Alkhorshid, N.R., Araujo, G.L., Palmeira, E.M., 2018. Behavior of geosynthetic-encased stone columns in soft clay: numerical and analytical evaluations. Soils Rocks 41 (3), 333–343.

Alkhorshid, N.R., Araujo, G.L., Palmeira, E.M., 2019. Large-scale load capacity tests on a geosynthetic encased column. Geotext. Geomembranes 47 (5), 632–641.

Alkhorshid, N.R., Araujo, G.L., Palmeira, E.M., 2020. Large scale tests on geotextile encased stone columns. In: GeoAmericas2020 – Proceedings of the 4th Pan-American Conference on Geosynthetics. Rio de Janeiro, Brazil.

Alkhorshid, N.R., Nalbantoglu, Z., Araujo, G.L., 2014. 3D analysis of full scale stone column reinforced soft clay: numerical evaluation. In: Proceedings of the 17th Brazilian Congress of Soil Mechanics. Cobramseg, Goiânia, Brazil.

Almeida, M.S., Hosseinpour, I., Riccio, M., 2013. Performance of a geosynthetic-encased column (GEC) in soft ground: numerical and analytical studies. Geosynth. Int. 20 (4), 252–262.

Araujo, G.L., Palmeira, E.M., Cunha, R.P., 2009. Behaviour of geosynthetic-encased granular columns in porous collapsible soil. Geosynth. Int. 16 (6), 433–451.

Castro, J., Karstunen, M., 2010. Numerical simulations of stone column installation. Can. Geotech. J. 47 (10), 1127–1138.

Castro, J., Sagaseta, C., 2011. Deformation and consolidation around encased stone columns. Geotext. Geomembranes 29 (3), 268–276.

Castro, J., Sagaseta, C., 2013. Influence of elastic strains during plastic deformation of encased stone columns. Geotext. Geomembranes 37, 45–53.

Cengiz, C., Guler, E., 2020. Load bearing and settlement characteristics of geosynthetic encased columns under seismic loads. Soil Dynam. Earthq. Eng. 136, 106244.

Chen, J.F., Li, L.Y., Zhang, Z., Zhang, X., Xu, C., Rajesh, S., Feng, S.Z., 2020. Centrifuge modeling of geosynthetic-encased stone column-supported embankment over soft clay. Geotext. Geomembranes 49 (1), 210–221.

De Mello, L.G., Mondolfo, M., Montez, F., Tsukahara, C.N., Bilfinger, W., 2008. First use of geosynthetic encased sand columns in South America. In: Proceedings of the 1st Pan-American Geosynthetics Conference, pp. 1332–1341.

Gäb, M., Schweiger, H.F., Pietraszewska, D.K., Karstunen, M., 2008. Numerical analysis of a floating stone column foundation using different constitutive models. In: Proceedings of the 2nd International Workshop on the Geotechnics of Soft Soils – Focus on Ground Improvement, Glasgow.

Gholaminejad, A., Mahboubi, A., Noorzad, A., 2020. Encased stone columns: coupled continuum–discrete modelling and observations. Geosynth. Int. 27 (6), 581–592.

Gniel, J., Bouazza, A., 2009. Improvement of soft soils using geogrid encased stone columns. Geotext. Geomembranes 27 (3), 167–175.

Goughnour, R.R., Bayuk, A.A., 1979. Analysis of stone column-soil matrix interaction under vertical load. In: Proceedings of the International Conference on Soil Reinforcement: Reinforced Earth and Other Techniques.

Gu, M., Zhao, M., Zhang, L., Han, J., 2016. Effects of geogrid encasement on lateral and vertical deformations of stone columns in model tests. Geosynth. Int. 23 (2), 100–112.

Hong, Y.S., Wu, C.S., Kou, C.M., Chang, C.H., 2017. A numerical analysis of a fully penetrated encased granular column. Geotext. Geomembranes 45 (5), 391–405.

Hosseinpour, I., Riccio, M., Almeida, M.S., 2014. Numerical evaluation of a granular column reinforced by geosynthetics using encasement and laminated disks. Geotext. Geomembranes 42 (4), 363–373.

Hosseinpour, I., Soriano, C., Almeida, M.S., 2019. A comparative study for the performance of encased granular columns. J. Rock Mech. Geotech. Eng. 11 (2), 379–388.

Keykhosropur, L., Soroush, A., Imam, R., 2012. 3D numerical analyses of geosynthetic encased stone columns. Geotext. Geomembranes 35, 61–68.

Khabbazian, M., Kaliakin, V.N., Meehan, C.L., 2010. Numerical study of the effect of geosynthetic encasement on the behaviour of granular columns. Geosynth. Int. 17 (3), 132–143.

Li, L.Y., Rajesh, S., Chen, J.F., 2020. Centrifuge model tests on the deformation behavior of geosynthetic-encased stone column supported embankment under undrained condition. Geomembranes 49 (3), 550–563.

Mohapatra, S.R., Rajagopal, R., Sharma, J., 2017. 3-dimensional numerical modeling of geosynthetic-encased granular columns. Geotext. Geomembranes 45 (3), 131–141.

Murugesan, S., Rajagopal, K., 2007. Model tests on geosynthetic-encased stone columns. Geosynth. Int. 14 (6), 346–354.

Murugesan, S., Rajagopal, K., 2010. Studies on the behavior of single and group of geosynthetic encased stone columns. J. Geotech. Geoenviron. Eng. 136 (1), 129–139.

Nagula, S.S., Nguyen, D.M., Grabe, J., 2018. Numerical modelling and validation of geosynthetic encased columns in soft soils with installation effect. Geotext. Geomembranes 46 (6), 790–800.

Oh, E.Y., Balasubramaniam, A.S., Surarak, C., Bolton, M., Chai, G.W., Huang, M., Braund, M., 2007. Behaviour of a highway embankment on stone columns improved estuarine clay. In: Proceedings of the 16th Southeast Asian Geotechnical Conference.

Priebe, H.J., 1995. Design of vibro replacement. Ground Eng. 28 (10), 31–37.

Pulko, B., Logar, J., 2017. Fully coupled solution for the consolidation of poroelastic soil around geosynthetic encased stone columns. Geotext. Geomembranes 45 (6), 616–626.

Rajesh, S., 2017. Time-dependent behaviour of fully and partially penetrated geosynthetic encased stone columns. Geosynth. Int. 24 (1), 60–71.

Rathod, D., Abid, M.S., Vanapalli, S.K., 2020. Performance of polypropylene textile encased stone columns. Geotext. Geomembranes 49 (1), 222–242.

Schanz, T., 1998. Zur modellierung des mechanischen verhaltens von reibungsmaterialen. PhD Thesis. Stuttgart Universität.

Schanz, T., Vermeer, P.A., Bonnier, P.G., 1999. The hardening soil model: formulation and verification. In: Beyond 2000 in Computational Geotechnics. PLAXIS International.

Sharma, R.S., Kumar, B.R., Ngendra, G., 2004. Compressive load response of granular piles reinforced with geogrids. Can. Geotech. J. 41, 187–192.

Walker, R., Indraratna, B., 2006. Vertical drain consolidation with parabolic distribution of permeability in smear zone. J. Geotech. Geoenviron. Eng. 132 (7), 937–941.

Wang, G., 2009. Consolidation of soft clay foundations reinforced by stone columns under time-dependent loadings. J. Geotech. Geoenviron. Eng. 135 (12), 1922–1931.

Weber, T., 2008. Modellierung der Baugrundverbesserung mit Schottersäulen. PhD Thesis. ETH Zurich.

Xue, J., Liu, Z., Chen, J., 2019. Triaxial compressive behaviour of geotextile encased stone columns. Comput. Geotech. 108, 53–60.

Yoo, C., Lee, D., 2012. Performance of geogrid-encased stone columns in soft ground: full-scale load tests. Geosynth. Int. 19 (6), 480–490.

Zhang, L., Xu, Z., Zhou, S., 2020. Vertical cyclic loading response of geosynthetic-encased stone column in soft clay. Geotext. Geomembranes 48 (6), 897–911.

Zhang, L., Zhao, M., Shi, C., Zhao, H., 2013. Settlement calculation of composite foundation reinforced with stone columns. Int. J. GeoMech. 13 (3), 248–256.

Zhang, Y., Chan, D., Wang, Y., 2012. Consolidation of composite foundation improved by geosynthetic-encased stone columns. Geotext. Geomembranes 32, 10–17.

Nima Rostami Alkhorshid obtained his BSc and MSc degrees in Civil Engineering from the Azad Shushtar University (Iran) in 2007 and Eastern Mediterranean University (Cyprus) in 2012, respectively, and his PhD in Geotechnical Engineering from the University of Brasília (Brazil) in 2017. He worked at Khuzestan Government Office (Iran) as the supervisor of the Earthworks and paving projects. He is currently a geotechnical engineering and engineering geology professor at the Federal University of Itajubá-Campus Itabira since 2017. His research interests include (1) Soil improvement, (2) Experimental and numerical studies in soil and rock mechanics, (3) Geosynthetics, (4) Slope stability, and (5) Foundations and excavations.